Linking Intermetallics and Zintl Compounds: An Investigation of Ternary Trielides (Al, Ga, In) Forming the NaZn₁₃ Structure Type

Karen J. Nordell and Gordon J. Miller*

Department of Chemistry, Iowa State University, Ames, Iowa 50011-3111

A populous group of ternary trielide rich (Al, Ga, In) intermetallics forming the $NaZn_{13}$ structure type has been synthesized from stoichiometric combinations of the elements in an arc melter. These ternary compounds have the general formula AM_xT_{13-x}, where A = Ba, Sr, La, Eu, M = Cu and Ag, and T = Al, Ga, and In, with $5 \leq x \leq 6.5$, and have been structurally characterized by both powder and single-crystal X-ray diffraction. Furthermore, magnetic susceptibility, electrical resistivity, XPS, and EDS measurements are reported for some of the samples. Single-crystal X-ray diffraction experiments on $BaCu_5Al_8$ ($BaCu_{5.10(7)}Al_{7.90(7)}$, cubic, $a = 12.205(4)$ Å, $Z = 8$) and $EuCu_{6.5}Al_{6.5}$ ($EuCu_{6.41(5)}Al_{6.59(5)}$, cubic, $a = 11.928(1)$ Å, $Z = 8$) indicate that the quasi-infinite three-dimensional $[Cu_xAl_{13-x}]$ framework involves mostly Cu atoms centering icosahedra, with its vertexes randomly occupied by the remaining Cu and Al atoms. On the other hand, when M = Ag, Al shows a greater tendency to occupy the center of the icosahedra. A systematic study of the compositional variation in $BaCu_xAl_{13-x}$ demonstrates that the $NaZn_{13}$ type phase exists within a narrow range of x between five and six. To examine the role of the cation A in stabilizing this structure, quaternary phases, e.g., $BaSrAg_{12}Al_{14}$ ($BaSrAg_{12.0(1)}Al_{14.0(1)}$, cubic, $a = 12.689(1)$ Å, $Z = 4$) and $SrCeCu_{12}Al_{14}$ ($SrCeCu_{11.74(2)}Al_{14.26(2)}$, cubic, $a = 11.938(1)$ Å, $Z = 4$), were prepared and characterized. Extended Hückel calculations on these ternary aluminides demonstrate how the tuning of the system's stoichiometry maximizes the bonding within the atom-centered icosahedral framework. These calculations also address the substitution pattern of M and T within the $[M_xT_{13-x}]$ network. Tight-binding LMTO calculations have also been applied to examine the charge-density and electron-localization functions (ELF) in this structure for different electron counts in order to address the nature of chemical bonding in these phases. One important conclusion from the theoretical results is that the $NaZn_{13}$ type phases show optimal stability for 40−42 valence electrons for the $[M_xT_{13-x}]$ framework.

Intermetallic compounds offer a rich collection of examples for detailed investigations of the relationship among composition, structure, and properties.[1] All three characteristics are fundamentally coupled to each other via the electronic structure of the material. To date, there are no general and simple models for the electronic structure of intermetallics—the difference in electronegativities, the numbers of valence atomic orbitals available and utilized in chemical bonding, and the propensity for large coordination numbers preclude the application of simple chemical bonding theories to interpret and rationalize many findings.[2] Nevertheless, the valence electron concentration per atom (vec) of an intermetallic compound has been shown to correlate with structure in some well-known classes of intermetallic compounds: Zintl compounds,[3] Hume−Rothery phases,[4] and Laves phases,[1] to name three. In this paper, we concentrate our attention on relationships between the first two classes.

Eduard Zintl is well-known for studying the structures of compounds formed between electropositive metals and main-group elements, in which the electropositive metal atoms formally donate their valence electrons to the main-group atoms, whose network is determined by simple electron counting rules.[5] The vec values for these phases are calculated from the total number of valence electrons, but with respect to the main-group atoms forming the covalently bonded network. Recent research has focused on compounds whose major main-group constituents are atoms at the so-called Zintl border,[6] which separates groups 13 and 14, because, in combination with electropositive metals, the elements in and to the right of group 14 form structures which can be rationalized using the octet rule (the connectivity equals $8 - N$, where N is the number of valence electrons assigned to the element), whereas the group 13 elements generally do not. Elements to the right of the Zintl border usually form valence compounds, which are electron-precise compounds with narrow ranges of composition, and whose electronic structures are consistent with filled bonding, filled nonbonding, and empty antibonding levels. For such compounds, vec is ≥ 4. On the other hand, many compounds with elements to the left of the Zintl border cannot be classified by any simple electron-counting rules, but behave like traditional intermetallic compounds with small heats of formation and wide ranges of homogeneity for different structures. The electronic structures

(1) (a) Pearson, W. B. *The Crystal Chemistry and Physics of Metals and Alloys*; Wiley-Interscience: New York, 1972. (b) *Intermetallic Compounds*; Westbrook, J. H., Ed.; John Wiley & Sons: New York, 1967. (c) Ferro, R.; Saccone, A. In *Materials Science and Technology*; Gerold, V., Ed.; VCH: Weinheim, 1993; Vol. 1, p 123.
(2) Burdett, J. K. *Molecular Shapes*; Wiley: New York, 1980.
(3) Nesper, R. *Prog. Solid State Chem.* **1990**, *20*, 1 and references therein.
(4) Pettifor, D. G. *Bonding and Structure of Molecules and Solids*; Clarendon Press: Oxford, 1995.

(5) (a) Zintl, E.; Dullenkopf, W. *Z. Phys. Chem., Abt. B* **1932**, *B16*, 183. (b) Zintl, E.; Brauer, G. *Z. Phys. Chem., Abt. B* **1933**, *B20*, 245. Zintl, E. *Angew. Chem.* **1939**, *52*, 1.
(6) Miller, G. J. In *Chemistry, Structure, and Bonding of Zintl Phases and Ions*; VCH Publishers: New York, 1996; p 1 and references therein.

of these types of compounds have not been investigated, in general, with respect to chemical-bonding aspects.

While classical Zintl phases are intermetallics whose metallic components come from opposite sides of the periodic table, e.g., NaTl, the Hume−Rothery phases are intermetallic compounds composed of late-transition metals (groups 8−12) through the post-transition metals, i.e., CuZn or Cu_3Sn.[7] Hume−Rothery observed that certain structure types formed with narrow ranges of vec between one and two: for example, the β-brass structure (bcc) occurs for vec = 1.50, the γ-brass structure exists for vec = 1.61, and ϵ-phases (hcp) are observed when vec = 1.75.[8] To count valence electrons in these phases, the valence d-orbital electrons are not included. While the Hume−Rothery phases correlate certain structures with vec values between 1 and 2, and the Zintl−Klemm-Busmann rules[9] account for the structures of certain compounds where the vec exceeds 4, there are no clear classification schemes for the range $2 \leq vec \leq 4$. Thus, our interest is directed toward an understanding of the structural, chemical, and physical ramifications of intermetallic compounds "between" Hume−Rothery and Zintl phases.

Many binary and ternary intermetallic compounds in which a group 13 metal (Al, Ga, In, Tl; called trielides[10]) is a major component have a vec near 3. While many of these intermetallics are not easily classified by any set of simple counting rules, this has not discouraged extensive synthetic efforts and structural characterization of new binary and ternary phases containing them. In particular, the most populous group of ternary aluminides reported in *Pearson's Handbook of Crystallographic Data for Intermetallic Phases* and forming a single structure type is the $ThMn_{12}$ structure type.[11] Many rare earth (Ln), transition metal (T) aluminides with the general formula LnT_xAl_{12-x} (where $4 < x < 6$; Ln = Y, Ce − Lu, Th, U; T = Cr, Mn, Fe, Cu) have been identified in this tetragonal variant of $CaCu_5$.[12−14] Most of the ternary compounds in which Cu is the transition metal have vec values between 2 and 2.5, and therefore fall well within the vec region of our interest.

We have begun our research with ternary systems in which the three components are a true blend of both Zintl and Hume−Rothery phases, including an electropositive alkaline earth metal, a late transition metal, and a trielide metal (Al, Ga, In). The first of these compounds we reported was $BaCu_5Al_8$, which forms the $NaZn_{13}$ structure type, in which the Ba atoms are surrounded by a network of interconnected, atom-centered icosahedra composed of copper and aluminum atoms. Several MCu_xAl_{13-x} (M = Ca, Sr, La, Ce, Pr, Nd, Sm, Eu; $5 < x < 7$) compounds have been reported with the $NaZn_{13}$ structure.[15,16]

To our knowledge, however, a systematic and detailed examination of these compounds has not been reported. In this paper we report the results of our investigation of the composition, structure, phase width, and electronic structure of many ternary aluminides which form the $NaZn_{13}$ structure type. A further aspect of this investigation is to explore and elucidate how different metallic elements are arranged in an intermetallic structure. Numerous structural studies have been limited to X-ray powder diffraction, which does not provide sufficient data to analyze this differentiation. We have recently shown that there are two energetic aspects that affect how elements "choose" sites in chemical structures: (1) minimization of the site potential and (2) maximization of the attractive two-center bonding interactions.[17] For many compounds, both factors contribute in parallel with each other, leading to the lowest energy arrangement. However, $CaLi_xAl_{2-x}$ shows partial segregation of both Li and Al atoms within the same network, to produce the lowest energy configuration—in this case the two terms counteract each other as Al begins to show aspects of a Zintl ion.[17,18]

Experimental Section

Synthesis. The synthesis of the trielide phases was carried out in a water-cooled, argon-filled arc melter. The samples were prepared from the elements in an argon-filled glovebox using Al foil as a wrapping, which served to keep the smaller pieces of metal or powder contained within the sample for arc melting as well as to keep the more reactive metals protected from air exposure as the samples were quickly transferred from the glovebox into the furnace chamber. The elements were used as supplied from the following sources: Ba and Sr rod (Johnson-Matthey, 99.5%), Cu (Johnson-Matthey, 99.5%), Ag powders (Alfa, 99.9%), Au wire (Aesar, 99.95%), Ga ingots (Alfa, 99.99%), In ingots (Alfa, 99.999%), Sn shot (Balzers 99.99%), rare earth ingots (Y, La, Ce, Sm, Eu, Gd, Tb, Dy, Ho, Er, Yb) (Ames Lab Rare-Earth Metals Preparation Center, 99.0%), and Al foil and wire (Alfa, 99.9%). Table 1 contains a summary of various reactant compositions and synthetic results. During the arc-melting procedure, a titanium or zirconium pellet was heated prior to melting the reactant mixture to further purify the argon atmosphere. The buttons were inverted several times and remelted to improve homogeneous melting and mixing of the elements. The reactions involving gallium and indium were carried out in tube furnaces with the reactants loaded into alumina crucibles, which were then sealed in evacuated fused-silica jackets. The arc-melted buttons appeared silvery with a dulled luster on the outer surface, but the inner volume was very lustrous. The buttons were easily broken up into smaller pieces or ground into fine black powders for Guinier X-ray powder diffraction (XPD) patterns, which were taken immediately after arc welding to identify crystalline phases in the products. Samples were wrapped in Nb foil (0.025 mm, Alfa, 99.8%) and sealed in evacuated fused-silica tubes for annealing at temperatures ranging from 873 to 1373 K, depending on the compositions of the products. The Guinier XPD patterns for the annealed products contained sharper lines than the initial post arc-melted patterns, which indicated an improved crystallinity of the product. However, the positions and relative intensities of the lines for most of the products did not change, to suggest no change in the structure upon annealing. XPD patterns observed from products ground and handled exclusively in the glovebox were identical to those of products handled in the air. The exposed surfaces are assumed to be passivated instantaneously, and complete oxidation of the bulk materials is not observed.

Single-crystal data were collected on crystals selected from both annealed and unannealed products. Crystals were generally covered with epoxy and attached to glass fibers in air, but many crystals were loaded into capillaries in the glovebox. All of the single crystals chosen had an irregular shape and a silvery luster. After a satisfactory single-

(7) Hume−Rothery, W. *J. Inst. Met.* **1926**, *35*, 295.
(8) (a) Hume−Rothery, W. *The Metallic State*; Clarendon: Oxford, 1931. (b) Hume−Rothery, W.; Raynor, G. V. *The Structures of Metals and Alloys*, 1st ed.; The Institute of Metals: London, 1936.
(9) (a) Schäfer, H.; Eisenmann, B.; Müller, W. *Angew. Chem., Int. Ed. Engl.* **1973**, *12*, 694. (b) Schäfer, H.; Eisenmann, B. *Rev. Inorg. Chem.* **1981**, *3*, 29. (c) Schäfer, H. *Annu. Rev. Mater. Sci.* **1985**, *15*, 1.
(10) Hulliger, F. In *Structure and Bonding in Crystals*, Vol. II; O'Keeffe, M., Navrotsky, A., Eds.; Academic Press: New York, 1981; p 297.
(11) Villars, P.; Calvert, L. D. *Pearson's Handbook of Crystallographic Data for Intermetallic Phases*, 2nd ed.; ASM International: Metals Park, OH, 1991.
(12) Felner, I.; Nowik, I. *J. Phys. Chem. Solids* **1979**, *40*, 1035.
(13) Felner, I. *J. Less-Common Met.* **1980**, *72*, 241.
(14) Buschow, K. H. J.; Van Hucht, J. H. N.; Van Den Hoogenhof, W. W. *J. Less-Common Met.* **1976**, *50*, 145.
(15) Shoemaker, D.; Marsh, R.; Ewing, F.; Pauling, L. *Acta Crystallogr.* **1952**, *5*, 637.
(16) (a) Cordier, G.; Czech, E.; Ochmann, H.; Schäfer, H. *J. Less-Common Met.* **1984**, *99*, 173. (b) Cordier, G.; Czech, E.; Schäfer, H. *J. Less-Common Met.* **1985**, *108*, 225. (c) Cordier, G.; Czech, E.; Schäfer, H.; Woll, P. *J. Less-Common Met.* **1985**, *110*, 327.

(17) Miller, G. J. *Eur. J. Inorg. Chem.* **1998**, 523.
(18) Nesper, R.; Miller, G. J. *J. Alloys Compds.* **1993**, *197*, 109.

Table 1. Reaction Compositions, Heating Methods, and Product Identification for Various Ternary Trielides, the Synthetic Goal Being the NaZn$_{13}$ Structure Type

reaction stoichiometry (target product)	heating method	reaction products[a]
BaAl$_{13}$	arc welder	BaAl$_4$ + Al
BaCuAl$_{12}$	arc welder	BaAl$_4$ + Al + BaCu$_5$Al$_8$(tr)[b]
BaCu$_3$Al$_{10}$	arc welder	BaCu$_5$Al$_8$ + CuAl$_2$ + Al
BaCu$_4$Al$_9$	arc welder	BaCu$_5$Al$_8$
BaCu$_5$Al$_8$	furnace (1393 K) and arc welder	BaCu$_5$Al$_8$[c]
BaCu$_6$Al$_7$	furnace (1398 K) and arc welder	BaCu$_6$Al$_7$[c]
BaCu$_9$Al$_4$	arc welder	BaCu$_6$Al$_7$ + Cu
BaCu$_{13}$	arc welder	BaCu$_{13}$
BaCu$_5$Ga$_8$	furnace (873 K, 1223 K)	BaCu$_6$Ga$_7$ + Ga + CuGa$_2$
BaCu$_5$In$_8$	furnace (873 K, 1223 K)	BaCu$_6$In$_7$ + In
BaAg$_3$Al$_{10}$	arc welder	BaAg$_5$Al$_8$ + Al
BaAg$_5$Al$_8$	arc welder	BaAg$_5$Al$_8$[c] + Al(tr)[b] + BaAl$_4$(tr)[b]
BaAg$_{5.5}$Al$_{7.5}$	arc welder	BaAg$_{5.5}$Al$_{7.5}$[c]
BaAg$_7$Ga$_6$	furnace (1273 K)	BaAg$_x$Ga$_{13-x}$ + BaGa$_4$
BaAg$_6$In$_7$	furnace (1273 K)	BaAg$_x$In$_{13-x}$ + In
SrCu$_5$Al$_8$	arc welder	SrCu$_6$Al$_7$[c] + CuAl$_2$
SrCu$_6$Al$_7$	arc welder	SrCu$_6$Al$_7$[c]
SrCu$_7$Al$_6$	arc welder	SrCu$_7$Al$_6$
SrAg$_5$Al$_8$	arc welder	SrAg$_6$Al$_7$ + Al
SrAg$_{5.5}$Al$_{7.5}$	arc welder	SrAg$_{5.5}$Al$_{7.5}$
EuCu$_{6.5}$Al$_{6.5}$	arc welder	EuCu$_{6.5}$Al$_{6.5}$[c] + CuAl$_2$
LaCu$_5$Al$_8$	furnace (1125 °C)	LaCu$_6$Al$_7$[c] + LaAl$_4$

[a] All products identified by X-ray powder diffraction. [b] tr = trace amounts. [c] Single-crystal X-ray diffraction experiment also conducted and solved.

Table 2. Quaternary Reactant Compositions and Products Observed by Powder and Single-Crystal X-ray Diffraction

reaction stoichiometry (target product)	preannealed products	postannealed products	lattice param[a] (Å)
(a) BaSrCu$_{12}$Al$_{14}$	BaSrCu$_{12}$Al$_{14}$		a = 12.073(2)[a]
(b) BaSrAg$_{11}$Al$_{15}$	BaAg$_{5.5}$Al$_{7.5}$ + SrAg$_{5.5}$Al$_{7.5}$	BaSrAg$_{11}$Al$_{15}$	a = 12.627(1)[a]
(c) BaYCu$_{12}$Al$_{14}$	BaCu$_{5.5}$Al$_{7.5}$ + YCu$_5$Al$_7$[b]		
(d) BaDyCu$_{12}$Al$_{14}$	BaCu$_6$Al$_7$ + DyCu$_5$Al$_7$[b]		
(e) SrGdCu$_{10}$Al$_{16}$	SrCu$_6$Al$_7$ + GdCu$_4$Al$_8$[b]		
(f) SrCeCu$_{12}$Al$_{14}$	SrCeCu$_{12}$Al$_{14}$		a = 11.938(1)[a]
(g) BaEuAg$_{11}$Al$_{15}$	BaAg$_6$Al$_7$ + EuAg$_5$Al$_6$[c]	BaEuAg$_{11}$Al$_{15}$	a = 12.729(1)[a]
(h) SrEuAg$_{12}$Al$_{14}$	Sr$_x$Eu$_{2-x}$Ag$_{12}$Al$_{14}$ + EuAg$_5$Al$_6$[c] (trace)		
(i) EuYbAg$_{10}$Al$_{12}$	EuYbAg$_{10}$Al$_{12}$[a,c]		
(j) BaGdAg$_{11}$Al$_{15}$	BaAg$_6$Al$_7$ + Gd$_2$Ag$_7$Al$_{10}$[d]	BaGdAg$_{11}$Al$_{15}$	a = 12.764(3)[a]

[a] Lattice parameters for NaZn$_{13}$ type phases are listed. [b] Single-crystal solution. [c] ThMn$_{12}$ structure type. [d] BaCd$_{11}$ structure type. [e] Th$_2$Ni$_{17}$ structure type.

Table 3. Refined Lattice Parameters for Ternary Trielides Forming the NaZn$_{13}$ Structure Type

compstn	lattice param (Å)	compstn	lattice param (Å)
BaCu$_{5.1}$Cu$_{7.9}$	12.205(4)	BaAg$_6$In$_7$[a]	13.442(3)
BaCu$_6$Ga$_7$[a]	12.026(2)	SrCu$_{6.0}$Al$_{7.0}$	11.975(1)
BaCu$_6$In$_7$[a]	12.740(4)	SrAg$_{5.5}$Al$_{7.5}$[a]	12.605(6)
BaAg$_{5.8}$Al$_{7.2}$	12.666(3)	LaCu$_{5.9}$Al$_{7.1}$	11.952(4)
BaAg$_{6.0}$Ga$_{7.0}$	12.757(3)	EuCu$_{6.5}$Al$_{6.5}$	11.977(1)

[a] The composition is approximate for these compounds because the reaction product was not single-phase and a single-crystal X-ray structure refinement was not obtained.

crystal solution and refinement provided an estimated composition of the crystal, that composition was loaded for a subsequent reaction in an attempt to prepare single-phase material for physical-property measurements.

One important consideration in the synthesis and characterization of these intermetallics is the possibility of hydrogen and oxygen interstitials. These structures contain many tetrahedra where adventitious interstitial atoms could be located, and while our crystallographic experiments have not confirmed the presence of small atoms on any crystallographic site in these compounds, a small fraction of these sites could be occupied and not detected in the X-ray diffraction experiment. Any source of elemental aluminum is covered with an oxide coating, and elemental barium can be contaminated by as much as 20 atm % hydrogen. Therefore, to investigate the possibility of interstitial stabilization of these structures, the synthesis of BaCu$_5$Al$_8$ was carried out in a closed tantalum tube sealed within an evacuated fused-silica tube, using BaH$_2$ as a source of Ba atoms. With a short heating program up to 1273 K for a few hours, and then cooling slowly to 298 K, the reaction product did not contain any of the NaZn$_{13}$ type intermetallic phase. The same synthesis carried out with Ba metal as the source of Ba did yield BaCu$_5$Al$_8$ as the reaction product.

To test the role of the larger, cationic component, mixtures of two different electropositive metals (either two different alkaline earth elements or one alkaline earth and one rare earth element) were combined with the transition metal–aluminum mixture to form quaternary phases. Table 2 summarizes the attempted compositions and the synthetic results.

Structure Determination. Structural analyses of the products were carried out using both powder and single-crystal X-ray diffraction. X-ray powder diffraction patterns were collected at ambient temperature (ca. 295 ± 2 K) on an Enraf-Nonius Guinier camera using Cu Kα_1 radiation and Si as an internal standard. Lattice parameters were refined using the program FINAX and are listed in Table 3. Single-crystal data were collected on a Siemens P4 diffractometer at 298 ± 2 K using Mo Kα_1 radiation. Crystal quality was checked with rotation photographs and

profiles from photographically observed reflections to check peak shapes and widths. The unit cells of the single crystals were indexed from a set of 25–50 reflections in a 2θ range between 10° and 30°. Most data sets were collected with 2θ_{max} either 45° or 60°, the latter being used to refine mixed occupancies on a single site more precisely. Lorentz and polarization corrections were applied to all data sets, as well as semiempirical absorption corrections based on collected azimuthal scans. The structures were solved using direct methods, and refinement calculations were performed on a Digital Equipment Micro VAX 3100 computer with the SHELXTL-PLUS programs.[19] Table 4 contains relevant data-collection parameters and crystallographic results for BaCu$_5$Al$_8$, EuCu$_{6.5}$Al$_{6.5}$, and SrBaAg$_{12}$Al$_{14}$. Atomic positions, occupancy factors, and isotropic displacement parameters for these three phases are presented in Table 5. Table 6 lists a summary of single-crystal solutions for various ternary aluminide phases forming the NaZn$_{13}$ structure type in this investigation. Further details of these crystallographic studies are available from the authors upon request.

Physical Measurements. Magnetic-susceptibility measurements were conducted using a Quantum Designs SQUID magnetometer operated at 3 T between 6 and 300 K. After a diamagnetic core correction was applied to these data, BaCu$_5$Al$_8$ showed temperature-independent paramagnetism above 100 K (χ_{TIP} = 1.05(5) × 10^{-4} emu/mol), whereas EuCu$_{6.5}$Al$_{6.5}$ followed Curie–Weiss paramagnetism with an effective moment of 7.82(2) Bohr magnetons (T > 80 K), consistent with Eu^{2+} (spin-only moment = 7.94). The Weiss constant of +10 K for EuCu$_{6.5}$Al$_{6.5}$ suggests a weak ferromagnetic interaction between Eu^{2+} centers.

(19) (a) Sheldrick, G. M. In *Crystallographic Computing 3*; Sheldrick, G. M., Kruger, C., Goddard, R., Eds.; Oxford University Press: Oxford, 1985; p 185. (b) SHELXTL-93, Siemens Industrial Automation, Inc., Madison, WI.

(20) Shinar, J.; Dehmer, B.; Beaudry, B. J.; Peterson, D. T. *Phys. Rev. B: Condens. Matter* **1988**, *37*, 2066.

Table 4. Crystallographic Data from Single-Crystal X-ray Diffraction Measurements for $BaCu_5Al_8$, $EuCu_{6.5}Al_{6.5}$, and $SrBaAg_{12}Al_{14}$

	$BaCu_5Al_8$	$EuCl_{6.5}Al_{6.5}$	$SrBaAg_{12}Al_{14}$
refined compstn	$BaCu_{5.10(7)}$-$Al_{7.90(7)}$	$EuCu_{6.41(5)}$-$Al_{6.59(5)}$	$SrBaAg_{12.0(1)}$-$Al_{14.0(1)}$
form wt (g/mol)	674.5	737.2	1897.4
space group	$Fm\overline{3}c$ (No. 226)	$Fm\overline{3}c$ (No. 226)	$Fm\overline{3}c$ (No. 226)
a (Å)	12.205(4)	11.928(1)	12.689(1)
vol (Å^3)	1818.1(3)	1697.1(2)	2043.1(3)
Z	8	8	4
density (calc; g/cm^3)	4.977	5.768	6.158
abs coeff (cm^{-1})	166.67	236.11	162.54
wavelength (Å)	0.71073	0.71073	0.71073
temp (°C)	20(1)	20(1)	20(1)
residuals^a (all data)	$R = 0.0169$ $R_w = 0.0405$	$R = 0.0218$ $R_w = 0.0554$	$R = 0.0139$ $R_w = 0.0249$

^{a} $R = \sum||F_o| - |F_c||/\sum|F_o|$; $R_w = [\sum w(|F_o| - |F_c|)^2/\sum w(F_o)^2]^{1/2}$; $w = 1/\sigma^2(F_o)$.

Table 5. Positional Coordinates and Equivalent Isotropic Displacement Coefficients for $BaCu_5Al_8$, $EuCu_{6.5}Al_{6.5}$, and $SrBaAg_{12}Al_{14}$

atom	site	x	y	z	U_{eq}	site occ.
			$BaCu_5Al_8$			
Ba	8a	$1/4$	$1/4$	$1/4$	0.0072(5)	1.0
Cu1	8b	0	0	0	0.0148(5)	0.908(3)
Al1	8b	0	0	0	0.0148(5)	0.092(3)
Cu2	96i	0.1166(1)	0.1755(1)	0	0.0139(4)	0.349(6)
Al2	96i	0.1166(1)	0.1755(1)	0	0.0139(4)	0.651(6)
			$EuCu_{6.5}Al_{6.5}$			
Eu	8a	$1/4$	$1/4$	$1/4$	0.0082(4)	1.0
Cu1	8b	0	0	0	0.0107(9)	0.72(2)
Al1	8b	0	0	0	0.0107(9)	0.28(2)
Cu2	96i	0.117 13(9)	0.177 21(8)	0	0.0119(5)	0.474(8)
Al2	96i	0.117 13(9)	0.177 21(8)	0	0.0119(5)	0.526(8)
			$SrBaAg_{12}Al_{14}$			
Sr	8a	$1/4$	$1/4$	$1/4$	0.0099(4)	0.5
Ba	8a	$1/4$	$1/4$	$1/4$	0.0099(4)	0.5
Ag1	8b	0	0	0	0.0118(1)	0.149(6)
Al1	8b	0	0	0	0.0118(1)	0.851(6)
Ag2	96i	0.1226(1)	0.1807(1)	0.0	0.0133(3)	0.486(4)
Al2	96i	0.1226(1)	0.1807(1)	0.0	0.0133(3)	0.514(4)

Table 6. Summary of Single-Crystal Refinements on Various Ternary Aluminides Crystallizing in the $NaZn_{13}$ Structure Type

refined compstn	a (Å)	no. of reflctns collected	no. of unique reflctns	$2\theta_{max}$ (deg)	R, R_w (all data)
$BaCu_{5.10}Al_{7.90}$	12.205(4)	3496	117	60.0	0.0188, 0.0452
$BaCu_{5.51}Al_{7.49}$	12.168(1)	342	63	45.0	0.0179, 0.0290
$BaCu_{5.66}Al_{7.34}$	12.134(1)	560	128	60.0	0.0401, 0.0755
$BaCu_{6.09}Al_{6.91}$	12.084(1)	980	82	50.0	0.0219, 0.0542
$SrCu_{5.98}Al_{7.02}$	11.980(1)	466	110	60.0	0.0525, 0.0979
$LaCu_{5.89}Al_{7.11}$	11.965(1)	904	125	60.0	0.0217, 0.0416
$LaCu_{6.06}Al_{6.94}$	11.913(1)	324	61	45.0	0.0178, 0.0331
$EuCu_{5.96}Al_{7.04}$	11.940(1)	324	61	45.0	0.0173, 0.0355
$EuCu_{6.41}Al_{6.59}$	11.928(1)	894	124	60.0	0.0237, 0.0566
$BaAg_{5.59}Al_{7.41}$	12.677(1)	517	93	50.0	0.0239, 0.0506

Electrical resistivity measurements were carried out on $EuCu_{6.5}Al_{6.5}$ using the electrodeless "Q" method.[20] Data were collected between 100 and 300 K. The room-temperature resistivity was determined to be 120-(5) μOhm·cm, and at 100 K the value was 100(5) μOhm·cm. The data followed a nearly linear variation with temperature with a slope of 0.12 μOhm·cm/K.

X-ray photoelectron spectroscopic (XPS) measurements of core-binding energies and surface compositions were carried out using a PHI 5500 Multi-Technique Surface Analysis spectrometer. Surfaces of several products were initially analyzed as received without any

Table 7. XPS Data for $EuCu_6Al_7$ and $BaCu_5Al_8$ and Other Reference Materials

sample	element obsd	binding energy (eV)	ref	binding energy (eV)
Eu	Eu (3d$^{5/2}$)	1124.3	Eu (3d$^{5/2}$)	1125.6
Eu_2O_3	Eu (3d$^{5/2}$)	1133.5		
$EuAl_4$	Eu (3d$^{5/2}$)	1124.8		
$EuCu_6Al_7$	Eu (3d$^{5/2}$)	1124.7		
$BaCu_5Al_8$	Ba (3d$^{5/2}$)	779.8	Ba (3d$^{5/2}$)	779.3
$BaCu_5Al_8$	Cu (2p$^{3/2}$)	932.0	Cu (2p$^{3/2}$)	932.6
			$Cu_{64}Zn_{36}$ (2p$^{3/2}$)	932.6
$BaCu_5Al_8$	Al (2p)	72.0	Al (2p)	72.8
		74.3	Al_2O_3 (2p)	74.4

surface cleaning, which always showed an aluminum-rich oxide surface layer. These samples were subsequently sputtered with argon for several minutes to effectively expose "fresh" bulk sample. Table 7 presents the data collected on $NaZn_{13}$ type phases as well as some references for direct comparison of core-binding energies.

Scanning electron microscopy (SEM) and in situ energy dispersive spectroscopic (EDS) composition analysis were carried out in a JEOL 6100 Scanning Electron Microscope. Measurements were performed on powdered samples, crystals, and larger pieces of arc-melted buttons from both pre- and postannealed products. Since many of the products were a homogeneous mixture of two or more intermetallic phases, EDS was carried out just to identify the components in different products and not to provide a quantitative analysis of the product (i.e., no standards were used). In all cases, SEM and EDS confirmed the results of refinements from various single-crystal diffraction experiments. For example, SEM and EDS results from a cleaved surface of an arc-melted button of "$EuCu_5Al_7Sn$" showed large smooth surfaces of the sample which analyzed as only Eu, Cu, and Al combined with some smaller, rougher areas containing Eu, Cu, Al, and Sn. The X-ray powder pattern of this sample confirms the presence of $EuCu_6Al_7$ and elemental Sn.

Theoretical Calculations. The electronic structures of many actual and hypothetical ternary aluminides were calculated using the LCAO (tight-binding) approximation with the extended Hückel theory (EHT).[21] In $BaCu_5Al_8$, the Ba$-$(Cu/Al) distance is 3.576(1) Å. Due to this long distance and the diffuse nature of the atomic orbitals of the metals found on the Ba site, these atoms were not included in constructing the Hamiltonian matrix, but were considered to donate two electrons to the $[Cu_xAl_{13-x}]$ framework. In all calculations, a primitive unit cell containing 26 atoms was used, and integrations for Mulliken populations, overlap populations, total energies, densities of states, and crystal orbital overlap populations (COOP) curves[22] were carried out using a special points set[23] of 30K$-$50K points in the irreducible wedge of the first Brillouin zone. The random occupation of atoms in each icosahedron was modeled by considering several structures with different arrangements of copper and aluminum atoms and averaging the results. Atomic orbital parameters are as follows. Cu: 4s, single-ζ function, $\varsigma = 2.20$, $H_{ii} = -8.45$ eV; 4p, single-ζ function, $\varsigma = 2.20$, $H_{ii} = -2.98$ eV; 3d, double-ζ function, $\varsigma_1 = 5.95$, $c_1 = 0.5933$, $\varsigma_2 = 2.30$, $c_2 = 0.5744$ $H_{ii} = -10.94$ eV. Al: 3s, single-ζ function, $\varsigma = 1.37$, $H_{ii} = -12.30$ eV; 3p, single-ζ function, $\varsigma = 1.36$, $H_{ii} = -6.50$ eV.

Tight-binding linear muffin-tin orbital (TB-LMTO)[24] calculations were carried out on various ordered models of $BaCu_5Al_8$ and binary $NaZn_{13}$ type structures ($BaCu_{13}$, $BaZn_{13}$, and "$BaCuAl_{12}$") in order to examine the electron density and to evaluate the electron localization function (ELF) in this intermetallic system as the valence electron count

(21) (a) Hoffmann, R.; Lipscomb, W. N. *J. Chem. Phys.* **1962**, *36*, 2179, 3489. (b) Hoffmann, R. *J. Chem. Phys.* **1963**, *39*, 1397. (c) Ammeter, J. H.; Bürgi, H.-B.; Thibeault, J. C.; Hoffmann, R. *J. Am. Chem. Soc.* **1978**, *100*, 3686. (d) Whangbo, M.-H.; Hoffmann, R.; Woodward, R. B. *Proc. R. Soc. London, Ser. A* **1979**, *366*, 23.
(22) (a) Hughbank, T.; Hoffmann, R. *J. Am. Chem. Soc.* **1983**, *150*, 3528. (b) Wijeyesekera, S.; Hoffmann, R. *Organometallics* **1984**, *3*, 949.
(23) Chadi, D. J.; Cohen, M. L. *Phys. Rev. B: Condens. Matter* **1973**, *8*, 5747.
(24) (a) Andersen, O. K. *Phys. Rev. B: Condens. Matter* **1975**, *12*, 3060. (b) Skriver, H. L. *The LMTO Method*, Springer Ser. Solid-State Sci.; Springer: Berlin, 1984; Vol. 41. (c) Krier, G.; Jepsen, O.; Burkhardt, A.; Andersen, O. K. TB-LMTO-ASA version 47 under UNIX.
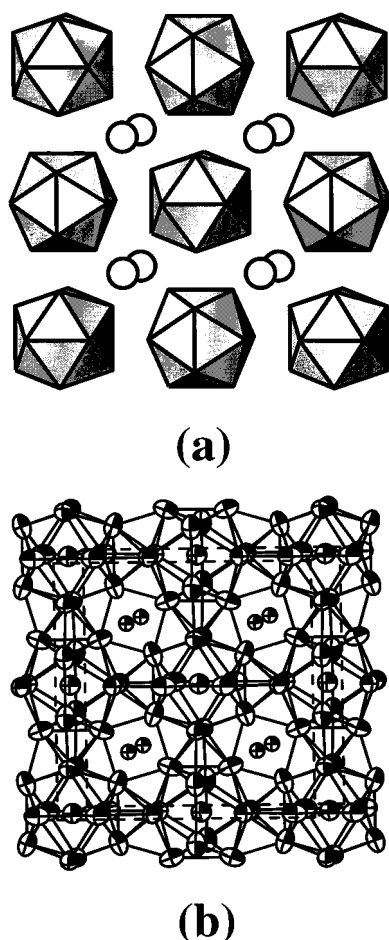
(a)

(b)

Figure 1. (001) slices of the NaZn$_{13}$ structure: (a) atom-centered icosahedral packing diagram with Na positions as large circles; (b) 99.9% displacement ellipsoids for BaCu$_5$Al$_8$ with interatomic distances shorter than 3.00 Å drawn.

changes. For these calculations, no empty spheres were needed to achieve convergence, and the overlap criterion between Wigner-Seitz spheres for atoms in the icosahedral network was set to a maximum of 20%. For the construction of the Hamiltonian, valence s, p, and d functions were used for Cu, Zn, and Al, while valence s and d functions were used for Ba.

Results and Discussion

The ternary and quaternary trielide phases reported in this paper form in the NaZn$_{13}$ type structure with the space group (No. 226),[11] but the ThMn$_{12}$ (*I4/mmm*), BaCd$_{11}$ (*I4$_1$/amd*), Th$_2$-Ni$_{17}$ (*P6$_3$/mmc*), Th$_2$Zn$_{17}$ (*R$\bar{3}$m*), ErZn$_5$ (*P6$_3$/mmc*), SrCo$_2$Al$_9$ (*P6/mmm*), and variations of the BaAl$_4$ (*I4/mmm*) structures have all been observed in ternary trielide systems.[25] In a forthcoming article we report the occurrences of these phases and examine their electronic structures.[26]

Structure Description. A (001) slice of the NaZn$_{13}$ structure is shown in Figure 1. The face-centered cubic unit cell contains 8 formula units (112 atoms; cF112[27]) which are distributed among three crystallographically nonequivalent positions (see Table 5). The large alkaline earth (Ba^{2+}, Sr^{2+}) or rare earth (La^{3+}, Eu^{2+}) cations (Wyckoff site 8a, point group *O*) are surrounded by 24-atom snub cubes, and a majority of the smaller

(25) Nordell, K. J. *Exploring Aluminum-Rich Intermetallics with Experiment and Theory*, Ph.D. Thesis, Iowa State University, 1997.
(26) Nordell, K. J.; Miller, G. M., to be published.
(27) The Pearson symbol[1] describes for a given structure its Laue symmetry, lattice class, and number of atoms in the unit cell.

A-Centered Snub Cube

Site Symmetry: O

T-Centered Icosahedron

Site Symmetry: T$_h$

Stella Quadrangula

Site Symmetry: D$_{2d}$

Figure 2. Three polyhedra that make up the NaZn$_{13}$ structure: snub cube, icosahedron, and stella quadrangula. Site symmetries for each polyhedron are indicated.

Table 8. Internuclear Distances (Å) in NaZn$_{13}$ type Phases: BaCu$_5$Al$_8$, EuCu$_{6.5}$Al$_{6.5}$, and SrBaAg$_{12}$Al$_{14}$

contacts	BaCu$_5$Al$_8$	EuCl$_{6.5}$Al$_{6.5}$	SrBaAg$_{12}$Al$_{14}$
8a−96i^a (24×)	3.5763(5)	3.4868(6)	3.6675(4)
8b−96i (12×)	2.5708(8)	2.5337(10)	2.7709(5)
96i−96i (intraicosahedral contacts)			
(4×)	2.6694(9)	2.6331(11)	2.8673(5)
(1×)	2.8462(8)	2.7943(10)	3.1113(5)
96i−96i (intericosahedral contacts)			
(2×)	2.6382(12)	2.556(2)	2.6027(7)
(2×)	2.7125(10)	2.630(2)	2.8161(8)

^{a} The three different crystallographic sites in this structure are: 8a (Ba, Eu, Sr); 8b (Cu, Ag, Al); and 96i (Cu, Ag, Al).

metal atoms (90% Cu in BaCu$_5$Al$_8$, 72% Cu in EuCu$_{6.5}$Al$_{6.5}$, and 85% Al in BaSrAg$_{12}$Al$_{14}$; Wyckoff site 8b, point group *T$_h$*) are surrounded by nearly regular icosahedra. These two sites together form the CsCl arrangement. The remaining atomic sites (Wyckoff site 96i), which involve a statistically random arrangement of Cu and Al or Ag and Al atoms, form the three-dimensional network of icosahedra that are interconnected by tetracapped tetrahedra (stella quadrangulae[28]) such that they are arranged in an alternate pattern along three mutually perpendicular directions. The three polyhedra which are, therefore, the structural building blocks for this structure type, i.e., the snub cube, the centered icosahedron, and the stella quadrangula are illustrated in Figure 2. This structure cannot be considered a true Frank-Kasper phase[29] because the snub cubes contain four-membered rings, and not every polyhedron involves a packing of tetrahedra.

Bond distances in the three compounds, BaCu$_5$Al$_8$, EuCu$_{6.5}$-Al$_{6.5}$, and BaSrAg$_{12}$Al$_{14}$, are listed in Table 8. The icosahedra, whose point symmetry is *T$_h$* (the highest allowed in crystallographic terms), have two different internuclear separations.

(28) Hyde, B. G.; Andersson, S. *Inorganic Crystal Structures*; Wiley-Interscience: New York, 1989.
(29) Barrett, C.; Massalski, T. B. *Structure of Metals*; Pergamon Press: Oxford, 1980.

Table 9. Refined Internuclear Distances (Å) and Site Occupations in Various Ternary ACu_xAl_{13-x} Phases Forming the $NaZn_{13}$ Structure Type

composition	site occupancy[a]	8a–96i (Å)	8b–96i (Å)	96i–96i (Å)
$BaCu_{5.10}Al_{7.90}$	$Ba(Cu_{0.91}Al_{0.09})$ $Ba[Cu_{4.19}Al_{7.81}]$	3.576(1)	2.571(1)	2.638(1) 2.669(1) 2.845(1)
$BaCu_{5.51}Al_{7.49}$	$Ba(Cu_{0.85}Al_{0.15})$ $Ba[Cu_{4.66}Al_{7.34}]$	3.565(1)	2.563(1)	2.630(1) 2.661(1) 2.837(1)
$BaCu_{5.66}Al_{7.34}$	$Ba(Cu_{0.84}Al_{0.16})$ $Ba[Cu_{4.82}Al_{7.18}]$	3.553(1)	2.560(1)	2.617(1) 2.657(1) 2.837(1)
$BaCu_{6.09}Al_{6.91}$	$Ba(Cu_{0.80}Al_{0.20})$ $Ba[Cu_{5.29}Al_{6.71}]$	3.537(1)	2.556(1)	2.601(1) 2.654(1) 2.825(1)
$SrCu_{5.98}Al_{7.02}$	$Sr(Cu_{0.61}Al_{0.39})$ $Sr[Cu_{5.37}Al_{6.63}]$	3.506(1)	2.537(1)	2.577(1) 2.638(1) 2.795(1)
$LaCu_{5.89}Al_{7.11}$	$La(Cu_{0.55}Al_{0.45})$ $La[Cu_{5.34}Al_{6.66}]$	3.498(1)	2.540(1)	2.565(1) 2.639(1) 2.804(1)
$LaCu_{6.06}Al_{6.94}$	$La(Cu_{0.49}Al_{0.51})$ $La[Cu_{5.57}Al_{6.43}]$	3.481(1)	2.533(1)	2.549(1) 2.630(1) 2.794(1)
$EuCu_{5.96}Al_{7.04}$	$Eu(Cu_{0.54}Al_{0.46})$ $Eu[Cu_{5.42}Al_{6.58}]$	3.494(1)	2.536(1)	2.563(1) 2.635(1) 2.797(1)
$EuCu_{6.41}Al_{6.59}$	$Eu(Cu_{0.72}Al_{0.28})$ $Eu[Cu_{5.69}Al_{6.31}]$	3.487(1)	2.534(1)	2.556(1) 2.631(1) 2.794(1)

[a] Atoms in parentheses, 8b sites; atoms in brackets, 96i sites.

According to the point symmetry of the cluster, 8 faces are regular triangles (perpendicular to the 3-fold rotation axes of the space group) and the remaining 12 faces are equivalent isosceles triangles with one long and two short distances (these two form the edges of the equilateral triangles). Although minor compositional variations do occur, which we shall discuss in a subsequent section, the spread in bond distances in the $[T_xAl_{13-x}]$ framework for all compounds with the same T show exceptionally small variations in bond distances, with the smallest separations indicating the greatest amounts of T in a particular ternary system. These variations are listed in Table 9.

From the viewpoint of atomic networks, the $NaZn_{13}$ structure can be built up from $[(3545)^2(3535)]$ two-dimensional nets (see Figure 3),[30] which is the arrangement of Hg atoms in Mn_2Hg_5.[30] For this net, Na atoms sit over the squares, while Zn atoms sit over all remaining pentagonal and trigonal sites.

Electronic Structure and Chemical Bonding. The structural features of these phases cause us to concentrate on the atom-centered icosahedra, which are interconnected via multicenter bonding. Results from EHT calculations, specifically the COOP curves in Figure 4 for various interatomic contacts in $BaCu_5$-Al_8, reveal that element–element bonding is nearly optimized within icosahedra, but not between them. Furthermore, the total DOS is essentially featureless near the Fermi level and may be considered to be nearly free-electron-like (also see Figure 4). The Cu 3d orbitals form a narrow band approximately 6 eV below the Fermi level, so we may treat Cu as a pseudo-one-electron main-group element in these intermetallics. These calculations have been repeated for numerous arrangements of Cu and Al on the icosahedral framework with no major differences in the features of these curves. A Mulliken population analysis shows that the atoms centering each icosahedron

(30) O'Keeffe, M.; Hyde, B. G. *Philos. Trans. R. Soc. London, Ser. A* **1980**, *295*, 553.
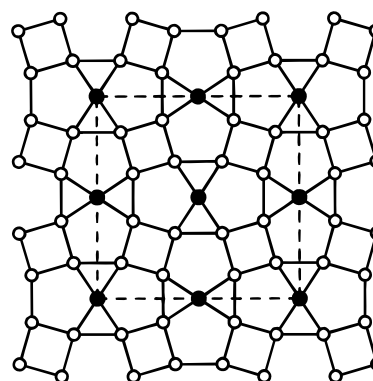
Figure 3. (001) projection of the $[(3545)^2(3535)]$ two-dimensional net at $z = 0$ in the $NaZn_{13}$ structure. Filled circles are 8b positions; open circles are 96i positions. (001) projection of the unit cell is given by dashed lines.
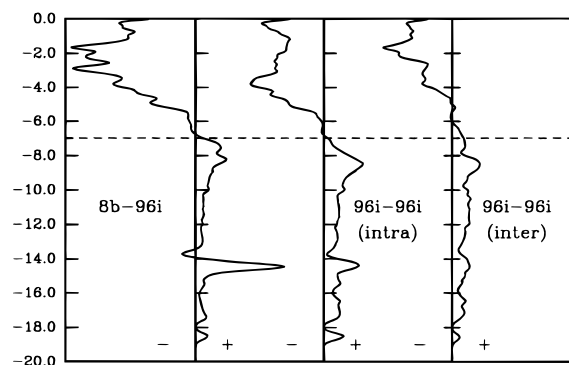
Figure 4. COOP curves for intra- and intericosahedral linkages in $BaCu_5Al_8$. The Fermi level is indicated by the dashed line. The leftmost curve is for the 8b–96i contact; the remaining two are for 96i–96i contacts. The two left curves are for intraicosahedral bonds; the rightmost curve is an average over all intericosahedral bonds (two types) less than 3.00 Å.

(the 8a sites) accumulate less charge (ca. 0.2–0.3 electrons) than the atoms on the icosahedra (the 96i sites). This result is consistent with Madelung calculations[31] on a homonuclear $[T_{13}]^{2-}$ net, for which the 8a site develops a negative ionic potential, i.e., a site for a cation.

To examine whether the specific COOP curves are fixed to the exact atomic orbital parameters and the exact composition $BaCu_5Al_8$, rigid-band calculations on the composition "$BaCuAl_{12}$" were performed for several different electron counts. The results, depicted in the COOP curves in Figure 5, indicate that optimal intraicosahedral bonding occurs for 40.5 electrons per formula unit with no energy gap at the Fermi level. This number of valence electrons is arrived at by treating the valence s, p, and d electrons of the metal at the 8a site (center of each icosahedron), while counting just the valence s and p electrons of the elements at the other two crystallographic sites. Therefore, $BaCu_5Al_8$ ($= Ba(Cu)[Cu_4Al_8]$) would have $(2 + 11 + 4 \times 1 + 8 \times 3) = 41$ valence electrons per formula unit. The composition which optimizes orbital overlap within the icosahedra corresponds to $BaCu_{5.25}Al_{7.75}$, which is close to our observed compositions. Therefore, according to an analysis of orbital-overlap populations, these ternary $NaZn_{13}$ type phases are electron-precise compounds with no band gap between occupied (bonding) and unoccupied (antibonding) orbitals.

The completely delocalized picture of the chemical bonding in these ternary icosahedral phases accounts well for the narrow

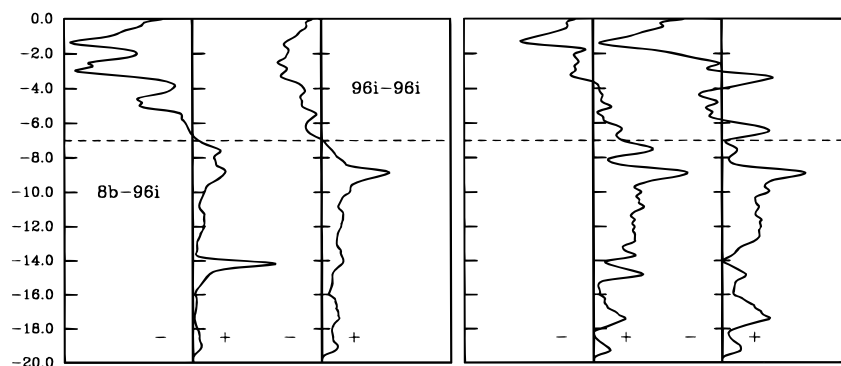(31) Seitz, F. *The Modern Theory of Solids*; Dover Publications: New York, 1987; Chapter 2.

Figure 5. COOP curves for (left) intra- and (right) intericosahedral linkages in "BaCuAl$_{12}$" with a Fermi level calculated for 40.5 valence electrons per formula unit (i.e., "BaCu$_{5.25}$Al$_{7.75}$").
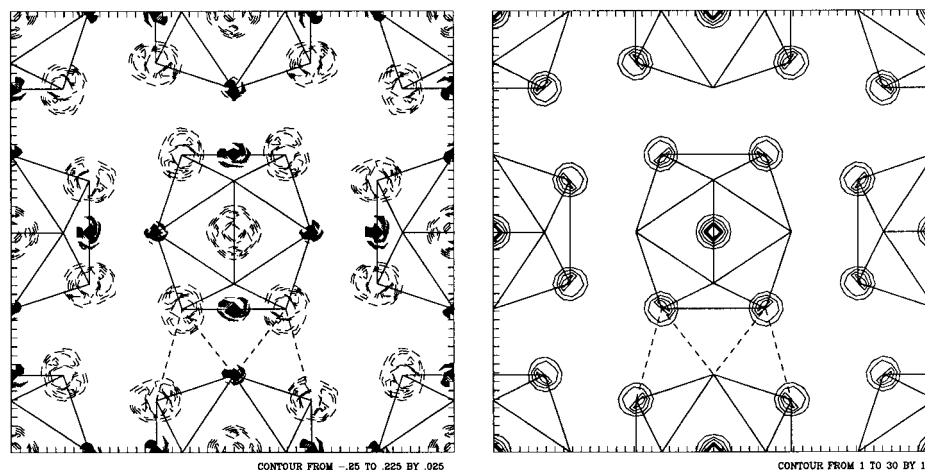

Figure 6. Contour diagrams of ELF (left) and the electron density distribution (right) for the $z = 0.00$ plane in BaCu$_{13}$. Projections of icosahedra and one stella quadrangula (dashed lines) are noted. ELF: contours plotted for values 0.25−0.75, solid lines for ELF ≥ 0.5; maxima occur at centers of the opposite edges in each icosahedron. Electron density: contours plotted for values 0.0−30.0; note the [(3545)^2(3535)] two-dimensional net.

range of valence-electron count for which the NaZn$_{13}$ type phase occurs. Chemists, however, also like to visualize the chemical bonding in compounds with respect to distribution of electron pairs, generally divided into classical two-center two-electron bonds and lone pairs. For intermetallic compounds and many cluster compounds, multicenter bonding is also necessary. The recent emergence of ELF (the electron localization function)[32] for the identification of "localized" electron pairs in structures involving inherently "delocalized" electrons may provide some additional insights into the nature of chemical bonding in intermetallics. With TB-LMTO calculations, we have calculated ELF values throughout the unit cell for BaCu$_{13}$, BaZn$_{13}$, and "BaCuAl$_{12}$", which have, respectively, 25, 38, and 49 valence electrons per formula unit. Figures 6−8 illustrate contour diagrams of the results: both ELF and electron density contours for a single plane parallel to (001) are presented; in the ELF plot, solid lines indicate ELF values exceeding the homogeneous gas value of 0.5, or, in other words, provide a visualization of where electron pairs tend to "localize" in each compound. For BaCu$_{13}$, there are pockets of ELF maxima (ELF$_{MAX}$ = 0.73) located near the centers of three pairs of opposite edges (the long edges) of each icosahedron at the 48f site (0.183, 0, 0). In fact, localization tends to occur within the stella quadrangulae linking two icosahedra together. In BaZn$_{13}$, the ELF maxima (ELF$_{MAX}$ = 0.62) are not as great as in BaCu$_{13}$ and now occur as new pockets over the 8 triangular faces of each icosahedron

that are perpendicular to the 3-fold axes at the 192j site (0.162, 0.207, 0.102). Thus, as vec increases in this intermetallic system, chemical-bonding effects change: in BaCu$_{13}$, homogeneous interactions within the icosahedron with stronger electron localization within the stella quadrangulae give way to more homogeneous bonding throughout BaZn$_{13}$ with small pockets of localization tied to some faces of each icosahedron. Finally, for the hypothetical compound "BaCuAl$_{12}$", the regions of high-electron localization become tubular and occur mostly within icosahedra.

The analysis using ELF parallels an orbital analysis for the two cases BaCu$_{13}$ and "BaCuAl$_{12}$". According to our structural description, the NaZn$_{13}$ type structure can be segmented into icosahedra and stella quadrangulae. Figure 9 illustrates molecular orbital diagrams for each polyhedron, using the appropriate valence atomic orbitals for the atoms involved. For BaCu$_{13}$, a [Cu(Cu′)$_{12}$] icosahedron utilizes 4s, 4p, 3d AO's at Cu and 4s, 4p AO's at Cu′; the stella quadrangulae are composed of only Cu′ atoms. For "BaCuAl$_{12}$", 4s, 4p, 3d AO's at Cu and 3s, 3p AO's at Al give the resulting diagrams, and the indicated "Fermi level" is for 41 valence electrons per formula unit. In BaCu$_{13}$, the 3d AO's of the central Cu are filled, along with the radial a$_g$ and t$_{1u}$ orbitals of the icosahedron. For the corresponding stella quadrangula, the four lowest bonding MO's are filled. Since there is a gap of ca. 1.95 eV, this orbital filling of 8 valence electrons exists as a possible "magic number" of electrons for this cluster.[33] Thus, as with the interpretation from ELF, BaCu$_{13}$ in the NaZn$_{13}$ structure creates strong bonding

(32) Savin, A.; Nesper, R.; Wengert, S.; Fässler, T. *Angew. Chem., Int. Ed. Engl.* **1997**, *36*, 1808.
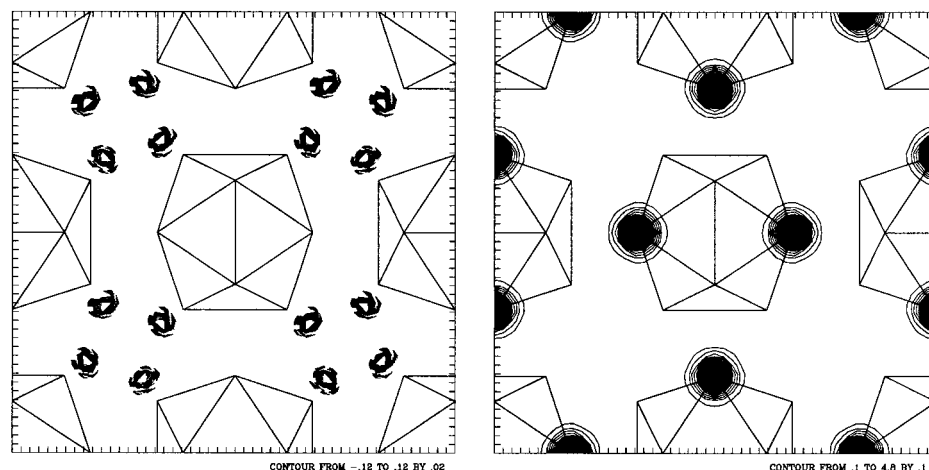
Figure 7. Contour diagrams of ELF (left) and the electron-density distribution (right) for the $z = 0.10$ plane in $BaZn_{13}$. Projections of icosahedra are noted. ELF: contours plotted for values 0.35−0.65, solid lines for ELF ≥ 0.5; maxima occur above eight of the faces of each icosahedron. Electron density: contours plotted for values 0.0−5.0; these center the pentagonal rings in the $[(3545)^2(3535)]$ two-dimensional net at $z = 0.00$.
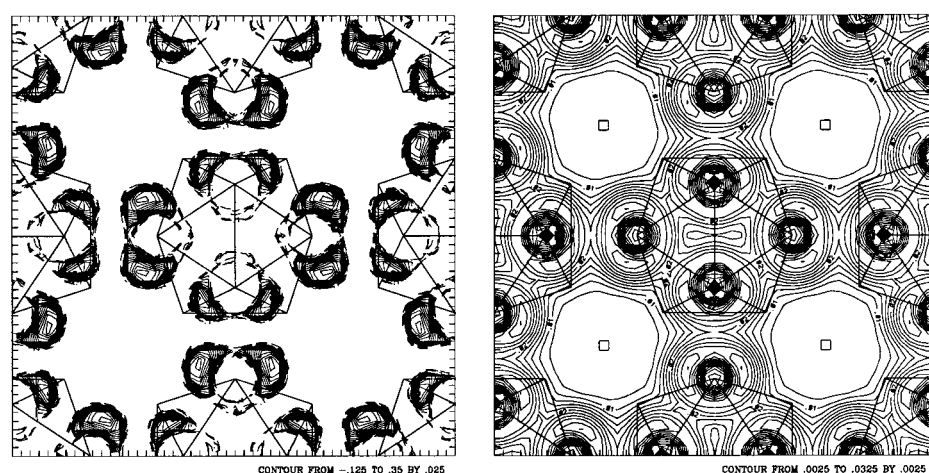

Figure 8. Contour diagrams of ELF (left) and the electron density distribution (right) for the $z = 0.15$ plane in "$BaCuAl_{12}$". Projections of icosahedra are noted. ELF: contours plotted for values 0.35−0.85, solid lines for ELF ≥ 0.5; maxima occur just outside the 24 shorter edges of each icosahedron. Electron density: contours plotted for values 0.0−0.05; the small values occur because the plane bisects two planes of atoms (at $z = 0.117$ and $z = 0.175$), and the maxima reflect these positions.

within the stella quadrangulae. On the other hand, for "$BaCu-Al_{12}$" 41 valence electrons fill the 3d AO's of the central Cu atom along with the radial a_g (2×; one inward-pointing cluster orbital that is bonding with the Cu 4s AO and the outward-pointing cluster orbital), t_{1u} and tangential h_g orbitals of the icosahedron. The additional eleven electrons occupy bands from the radial t_{1u} and tangential g_u and t_{1g} orbitals that are involved in intericosahedral bonding; these three orbitals lie close to the Fermi level. These three bands are weakly bonding within the icosahedron and account for the dispersion characteristics that lead to no energy gap between bonding and antibonding orbitals. The filling of these additional icosahedral orbitals shifts the ELF maxima away from the centers of the stella quadrangulae and toward the edges of the icosahedra, as we observed in going from $BaCu_{13}$ to $BaZn_{13}$. With respect to the stella quadrangula, all valence s orbitals are filled, and only some of the bonding p orbitals are occupied, in accord with the COOP curves of Figure 4 which compare intra- and intericosahedral bonding.

The Cations. For the EHT calculations, we considered the cations at the center of each snub cube to act as a classical cation. Since the electronegativity differences among Sr, Ba,

La, and Eu with Cu, Ag, Al, Ga, and In are not very large (Δ ~ 0.5−0.7 in Pauling units, which gives 6−12% ionic character[34]), this approximation may be poor. Therefore, we carried out XPS measurements to give us an indication of the nature of the electronic structure of the individual elements in these intermetallic phases. The data are summarized in Table 7. The reported binding energies have all been corrected for sample charging by setting the carbon reference peak to 284.8 eV. The Eu-containing phases (Eu, $EuAl_4$, and $EuCu_{6.5}Al_{6.5}$) all show identical binding energies for the Eu $3d^{5/2}$ and $3d^{3/2}$ peaks (1125.6 and 1154.4 eV, respectively) to suggest that each Eu atom donates two electrons to the conduction band. For $BaCu_5-Al_8$, which was sputtered with argon to "clean" the surface of any oxide before analysis, the binding energies for Ba suggest a very slightly oxidized Ba and slightly reduced Cu and Al atoms. Even with sputtering, however, there is still evidence of some Al_2O_3 on the surface of the sample.

TB-LMTO calculations were also performed using the complete structure in order to assess charge transfer within these intermetallics. Various arrangements of four Cu and eight Al aluminum atoms on the 96i sites were examined for a composition $BaCu_5Al_8$. On average in $BaCu_5Al_8$, Ba donates ap-

(33) (a) Martin, T. P.; Bergmann, T.; Göhlich, H.; Lange, T. *J. Phys. Chem.* **1991**, *95*, 6421. (b) Vajenine, G. V.; Hoffmann, R. *J. Am. Chem. Soc.* **1998**, *120*, 4200.

(34) Huheey, J. E. *Inorganic Chemistry: Principles of Structure and Reactivity*, 1st ed.; Harper and Row: New York, 1972.
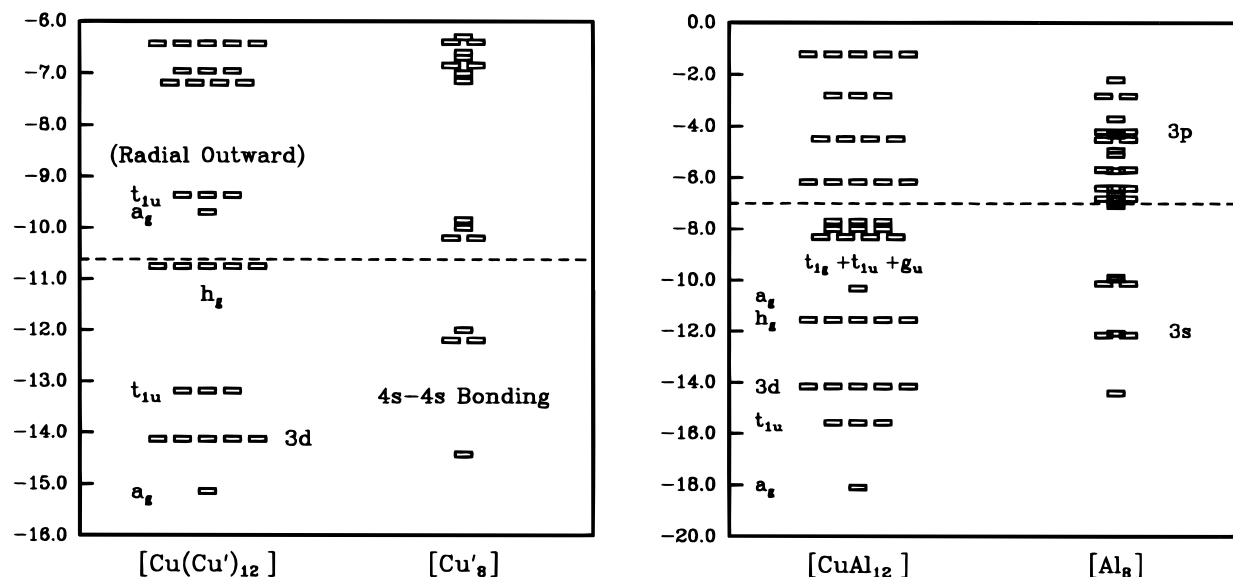
Figure 9. Molecular orbital energy diagrams for the icosahedron and the stella quadrangula in (left) BaCu₁₃ and (right) "BaCuAl₁₂" (Fermi level chosen for 41 valence electrons, as found in BaCu₅Al₈). Fermi levels are shown, and significant molecular orbitals are labeled. See text for further discussion.

proximately 0.25 electron to the three-dimensional [Cu₅Al₈] framework. Furthermore, the central Cu atom acquires ca. 0.4 electron, such that the 0.15 electron deficiency is spread among the icosahedral atoms. In effect, the TB-LMTO confirms our chemical intuition, in that the large cations contribute to the chemical bonding of the three-dimensional intermetallic framework by donating their valence electrons, as well as Pauling's ideas of electronegativity with respect to Cu, Al, and Ba. Further TB-LMTO calculations on BaZn₁₃ and BaCu₁₃ demonstrated charge transfer from Ba to the homonuclear network, with most of the negative charge going to the icosahedral atoms in BaZn₁₃ (i.e., $Ba^{+0.48}[Zn^0(Zn^{-0.04})_{12}]$), and the opposite effect happening in BaCu₁₃ ($Ba^{+0.81}[Cu^{-0.09}(Cu^{-0.06})_{12}]$).

Phase-Width Investigations. In the BaCu$_x$Al$_{13-x}$ system, a careful investigation of the phase width was carried out both synthetically and theoretically. Table 1 summarizes the results of efforts to synthesize single-phase product by varying the reaction composition for BaCu$_x$Al$_{13-x}$ from $0 \leq x \leq 13$. In all cases except $x = 4$, 5, and 6, multiple phases were observed in the X-ray powder diffraction patterns. BaCu₁₃ is reported to form the NaZn₁₃ structure,[11] although we could not confirm this. Using single-crystal X-ray diffraction and EDS, we considered the variation of composition within one arc-melted button by solving single-crystal data from many crystals loaded from the same product button. From a single arc-melted and annealed button with an initial composition of BaCu₅Al₈, three different crystals were analyzed by single-crystal X-ray diffraction and refined well with compositions of BaCu₅.₄₁₍₂₎Al₇.₅₉₍₂₎, BaCu₅.₄₈₍₁₎-Al₇.₅₂₍₁₎, and BaCu₅.₅₂₍₁₎Al₇.₄₈₍₁₎. These results support two important conclusions: (1) the ternary phases BaCu$_x$Al$_{13-x}$ have a narrow phase width between $5 < x < 6.2$, and (2) the composition within a certain product button is quite homogeneous. Other experiments were also carried out with EuCu$_x$Al$_{13-x}$ and LaCu$_x$Al$_{13-x}$ and gave similar results, except that the values of x were slightly different: for Eu, $5.9 < x < 6.5$; and for La, $5.8 < x < 6.2$.

These synthetic results in ternary A−Cu−Al systems nicely confirm the results of TB-LMTO and EHT calculations. We performed a series of calculations in which the Cu:Al ratio was varied from BaCu₁₃, "BaCu₁₂Al", ..., BaCu₅Al₈, BaCu₆Al₇, ..., "BaAl₁₃", and considered the total densities of states, Fermi

energies, and overlap populations for the icosahedral network. BaCu₁₃ and BaCu$_x$Al$_{13-x}$ ($5 < x < 6.2$) are known compounds, but the others are merely hypothetical compositions forming the NaZn₁₃ structure for the purpose of the calculations. Figure 10 contains three total DOS curves from TB-LMTO calculations for the three examples BaCu₁₃, BaCu₅Al₈, and "BaCuAl₁₂", with the Fermi energies represented by the dashed line. Each curve has a distinct Cu 3d band, which drops froms 3 to 6 eV below the Fermi level and progressively narrows as the Cu concentration decreases. Above this 3d band, the DOS is broad and nearly featureless in the three curves and follows a nearly free-electron-like distribution, i.e., parabolic variation with energy. The results from EHT calculations are qualitatively similar.[25]

Table 10 lists the Fermi energies, Mulliken populations, and a summary of overlap populations for this series of model compounds as calculated by EHT. As we have already pointed out, intraicosahedral bonding is optimized when the composition is close to BaCu₅.₅Al₇.₅. According to these results, the total number of valence electrons is near 40 per formula for the compositions BaCu₅Al₈ and BaCu₆Al₇. As we proceed to Cu rich compounds, the Fermi level drops (E_F for BaCu₁₃ is −10.62 eV), which leaves many bonding orbitals within the icosahedra unfilled. Furthermore, the number of valence electrons drops below 39 per formula unit. On the other hand, as the Al concentration increases, the Fermi level rises (for "BaCuAl₁₂" $E_F = −4.65$ eV), many antibonding states are filled, and the number of valence s and p electrons exceeds 32 per formula unit. For the compounds BaCu₅Al₈ and BaCu₆Al₇, the Fermi energy falls near this crossover between bonding and antibonding orbitals, and the number of valence electrons is near 40 per formula unit. Therefore, the NaZn₁₃ structure exists for systems showing approximately 40 valence electrons per AB₁₃ formula unit, and is stabilized by a Zintl type argument that interatomic bonding within the icosahedra is optimized by filling all bonding orbitals and leaving antibonding orbitals empty. Unlike the Zintl concept, however, is the occurrence of empty bonding orbitals for the stella quadrangulae which link these icosahedra together. In fact, our EHT and TB-LMTO calculations suggest that the electronic structure of the "extremely electron-deficient" BaCu₁₃ creates strong bonding within the stella quadrangulae and
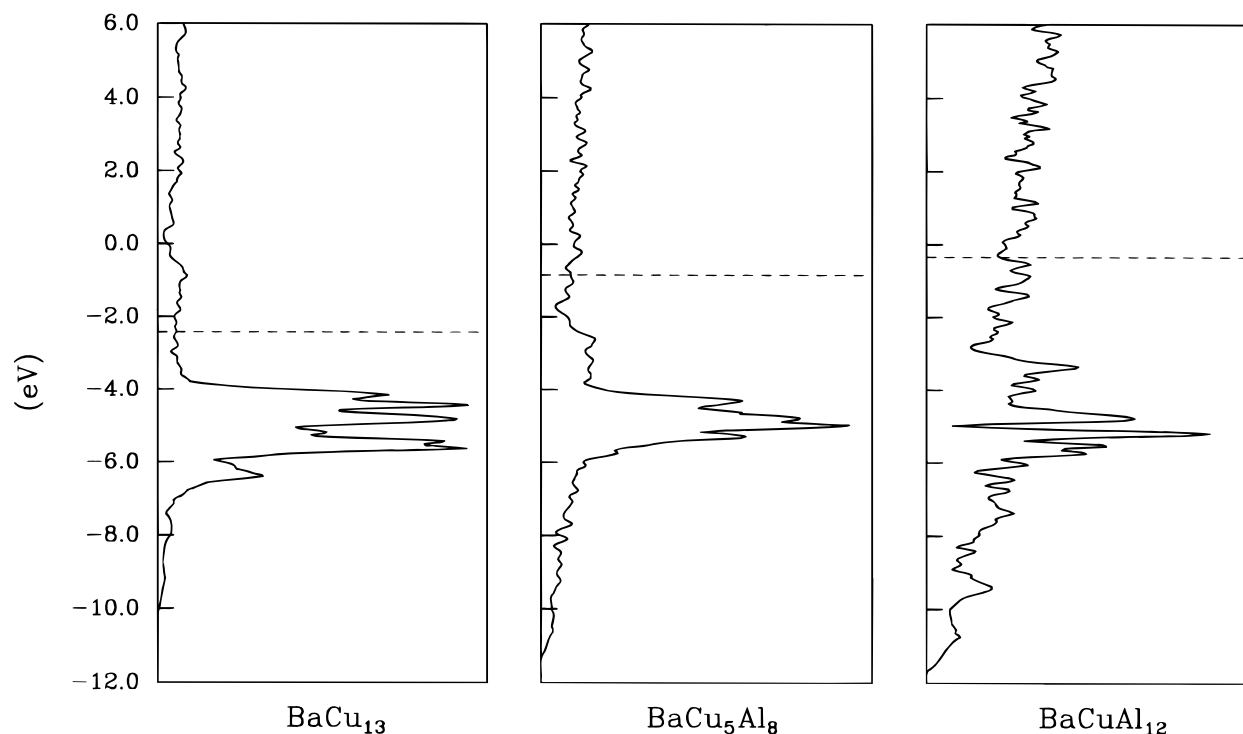
Figure 10. TB-LMTO total densities of states for (left) $BaCu_{13}$, (middle) $BaCu_5Al_8$, and (right) "$BaCuAl_{12}$". Fermi levels are shown. Note how the shape of the Cu 3d band changes with composition, as well as how its position changes with respect to the Fermi level. The shift is in accord with an increased reduction of Cu as its concentration drops in these intermetallic phases.

Table 10. Summary of EHT Computational Results for $BaCu_xAl_{13-x}$ ($1 \leq x \leq 13$), Including Calculated Fermi Levels (eV), Mulliken Populations for Each Subshell, Total Overlap Populations, and Total Number of Valence Electrons Per Formula Unit

compd	Fermi level (eV)	Mulliken populations		total overlap populations		total no. of valence electrons[b]
		(8b)[a]	(96i)[a]	(8b)−(96i)	(96i)−(96i)	
$BaCuAl_{12}$	−4.65 (9.898)	13.492	(Al) 2.959	0.1159	0.2352	49.000
$BaCu_3Al_{10}$	−6.00	12.309 (9.887)	(Cu) 12.747 (9.924) (Al) 2.720	0.1285	0.1995	45.155
$BaCu_4Al_9$	−6.45	12.124 (9.878)	(Cu) 12.452 (9.917) (Al) 2.612	0.1333	0.1463	43.247
$BaCu_5Al_8$	−7.03	12.012 (9.870)	(Cu) 12.245 (9.913) (Al) 2.501	0.1373	0.1462	41.348
$BaCu_6Al_7$	−7.33	11.835 (9.863)	(Cu) 12.040 (9.911) (Al) 2.424	0.1330	0.1454	39.448
$BaCu_7Al_6$	−7.73	11.719 (9.859)	(Cu) 11.885 (9.908) (Al) 2.329	0.1273	0.1386	37.555
$BaCu_8Al_5$	−8.06	11.537 (9.853)	(Cu) 11.758 (9.907) (Al) 2.231	0.1239	0.1488	35.649
$BaCu_1Cu_{12}$	−10.62	10.895 (9.807)	(Cu) 11.175 (9.860)	0.1285	0.1995	26.675

[a] Number in parentheses represents Mulliken population of Cu 3d orbitals. [b] Total no. of valence electrons = no. of spd valence electrons on 8b sites + no. of sp valence electrons on 96i sites.

homogeneous interactions within icosahedra. We address this problem in a subsequent paper.[26]

Ordering of Atoms on the Icosahedral Network. Our examination of the Ba−Cu−Al system in the NaZn$_{13}$ structure type never revealed any superstructure nor any ordering of Cu and Al among the 96 positions allocated to this site in the complete cubic unit cell. For $BaCu_5Al_8$, the 96i position is fractionally occupied by ca. 35% Cu and 65% Al, which gives an average composition of [Cu$_4$Al$_8$] for each icosahedron. For the other systems examined, the composition of the icosahedra

can vary between [T$_4$M$_8$] and [T$_6$M$_6$]. The question is how such a network of interconnected icosahedra is *colored*,[17] i.e., how do the two different types of atoms arrange themselves over the twelve icosahedral sites? For example, in the hypothetical compound "$BaCuAl_{12}$", if we stipulate Cu-centered icosahedra, there is only one *coloring* of the network, i.e., Cu atoms occupy the centers of the two icosahedra in the primitive cell, and Al atoms occupy all 24 icosahedral positions. If, however, the composition is $BaCu_5Al_8$, there is more than one way to *color* the icosahedra. For the composition BaCu[Cu$_4$Al$_8$], there are
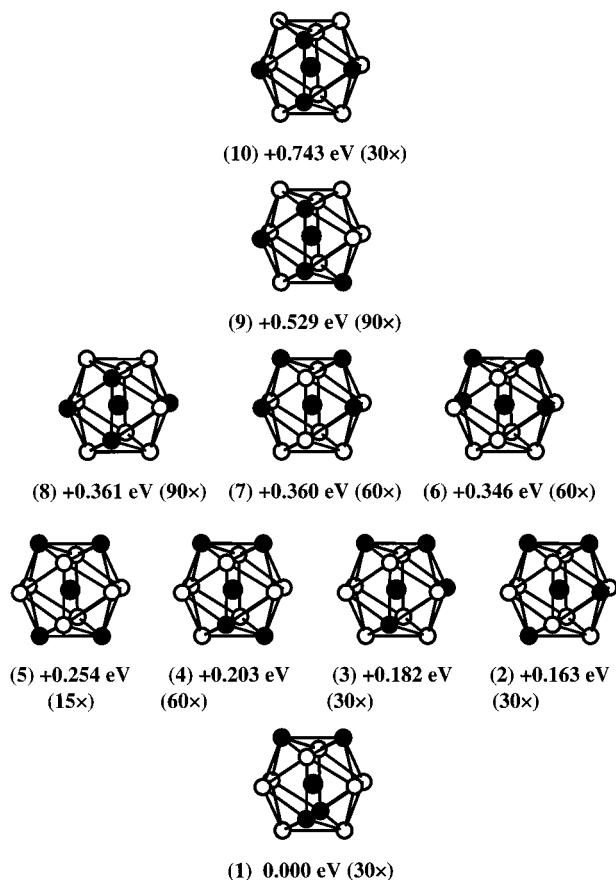
Figure 11. The 10 distinguishable (Cu)[Cu₄Al₈] icosahedral clusters shown from lowest to highest relative valence electron energy, as calculated by EHT. Cu atoms are filled circles; Al atoms are open circles. The clusters are also arranged with respect to the numbers of Cu–Cu, Al–Al, and Cu–Al contacts.

495 (= $12!/4! \times 8!$) different arrangements (not all of which are unique!) of Cu and Al on each icosahedron and eight icosahedra per unit cell to give ca. 3.6×10^{21} possible colorings of the three-dimensional network. Therefore, entropic effects at elevated temperatures certainly favor the disordered arrangement of atoms. Nevertheless, there may be enthalpic influences that limit the local structure of each icosahedron yet do not affect the crystallographic results. In the system $Ln_3Au_2Al_9$, we have demonstrated that partial disorder between Au and Al exists, but in a specific way due to repulsive Au–Au interactions.[35] Additionally, $CaLi_xAl_{2-x}$ demonstrates incomplete disorder due to both site-potential and orbital-overlap effects.[17,18]

Therefore, to investigate any enthalpic effects to the Cu and Al arrangement, we concentrated on the icosahedra, since the orbital overlap (chemical bonding) is optimized within these clusters in the $NaZn_{13}$ type construction. For the composition $Cu[Cu_4Al_8]$, Pólya's theorem[36] elucidates 10 unique ways to arrange these two sets of atoms on the vertices of the icosahedron.[37] Figure 11 illustrates these 10 arrangements: Cu atoms are shaded circles, Al atoms are open circles, and they are numbered from lowest to highest energy configurations for 42 valence electrons per cluster ($11 + 5 \times 1 + 8 \times 3 + 2$
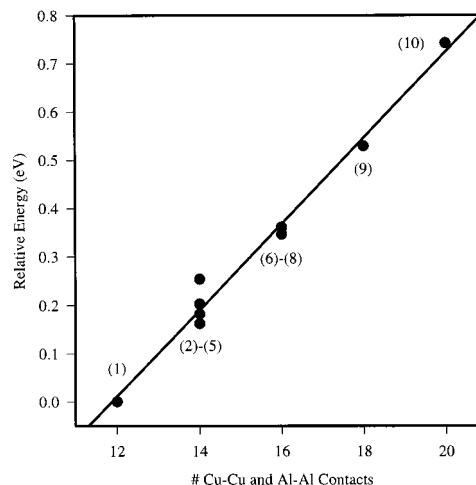
(35) Nordell, K. J.; Miller, G. J. *Angew. Chem., Int. Ed. Engl.* **1997**, *36*, 2008.
(36) McLarnan, T. J.; Moore, P. B. In *Structure and Bonding in Crystals*, Vol. II; O'Keeffe, M., Navrotsky, A., Eds.; Academic Press: New York, 1981; p 133.
(37) Teo, B. K.; Zhang, H.; Kean, Y.; Dang, H.; Shi, X. *J. Chem. Phys.* **1993**, *99*, 2929.

Figure 12. Plot of the energy variation in the 10 (Cu)[Cu₄Al₈] icosahedral clusters as the number of homoatomic contacts (Cu–Cu and Al–Al) varies within this set. Note the linear relationship.

electrons). Note that the lowest energy arrangement also has the fewest number of homoatomic (Cu–Cu and Al–Al) contacts in the polyhedron and the correspondingly highest number of heteroatomic (Cu–Al) contacts. Moreover, the difference in total energies between the lowest and highest energy configurations is just 0.743 eV per cluster (0.057 eV per atom), and the energies scale linearly with the number of homoatomic contacts (see Figure 12). If such clusters are forming during the synthesis in the melt at the temperatures in the arc melter, then there are at least five possible arrangements that can be significantly populated (0.18 eV corresponds to ca. 2100 K). We have also carried out various calculations on full three-dimensional structures using several different arrangements of these clusters and arrive at the same conclusions: the lowest energy configurations minimize the numbers of homoatomic Cu–Cu and Al–Al contacts in the network.[25]

From these *coloring* calculations, it is clearly more energetically favorable for the Cu atoms to be well separated from each other. The ultimate conclusion is to make the composition of each icosahedron near $Cu[Cu_4Al_8]$ in $BaCu_5Al_8$. However, the energy differences between colorings (1)−(5) in Figure 11 are small enough to assume that a mixture of several or all of these colorings contributes to the disorder observed in the X-ray diffraction experiment. In subsequent publications, we will report two new tetragonal variants of the $BaCu_5Al_8$ structure, $BaPd_4Al_9$[25,26] and $SrAu_6Al_6$,[25,26] in which there occurs partial ordering of the atoms on the icosahedral framework. The *coloring* of the network in $BaPd_4Al_9$ most closely resembles coloring (5) in Figure 11, whereas the empty 'Au_6Al_6' icosahedra in $SrAu_6Al_6$ are colored like numbers (1) and (3) in Figure 11, which are two of the lowest energy configurations.

Quaternary Phases. While $EuCu_{6.5}Al_{6.5}$ and $LaCu_6Al_7$ form the $NaZn_{13}$ structure, all the other rare earth elements, in combination with copper and aluminum in a nearly 1:13 ratio, form the $ThMn_{12}$ structure. The resemblance in both stoichiometry and elemental composition between the two groups of ternary intermetallic compounds forming either the $ThMn_{12}$ or $NaZn_{13}$ structure is striking! And yet, as prepared from the elements in the arc welder, no *ternary* combination of elements has yielded a product containing both structure types. Similar differences exist in the silver aluminides with $BaAg_{5.5}Al_{7.5}$ and $SrAg_{5.5}Al_{7.5}$ forming the $NaZn_{13}$ structure, but $LnAg_xAl_y$ compounds (with variable x and y) form other structures. For example, $EuAg_5Al_6$ forms the $BaCd_{11}$ structure type, and

$Ln_2Ag_xAl_{17-x}$ (Ln = La−Lu, except Eu and Yb) form either the Th_2Ni_{17} or Th_2Zn_{17} type depending on the silver:aluminum ratio.[25]

In an effort to examine this preference for either the $ThMn_{12}$ or $NaZn_{13}$ structure type, depending on the electropositive metal used, quaternary mixtures of elements were tested. Using the same experimental techniques described earlier, the synthesis of quaternary phases containing both a metal with a preference for the $ThMn_{12}$ structure and one with a preference for the $NaZn_{13}$ structure was carried out in the arc welder. Table 2 contains a list of these reactions. In most cases, the preannealed product was a mixture of two phases, while the postannealed product was single-phase. In the case of "$BaDyCu_{12}Al_{14}$", both the preannealed and postannealed (850 °C for 10 days) products were a combination of $BaCu_5Al_8$ and $DyCu_5Al_7$. However, in the case of $BaGdAg_{11}Al_{15}$, while the preannealed product was a mixture of phases, the postannealed product was single-phase with the $NaZn_{13}$ structure type.

The results of the reactions (a) $BaSrCu_{12}Al_{14}$ and (b) $BaSrAg_{12}Al_{14}$ in Table 2 are not surprising, since all four compounds $BaCu_5Al_8$, $SrCu_6Al_7$, $BaAg_5Al_8$, and $SrAg_6Al_7$ form the $NaZn_{13}$ structure. In the quaternary compound $BaSrCu_{12}Al_{14}$ ($a = 12.073(2)$ Å), barium and strontium atoms randomly occupy the centers of snub cubes at site 8b (1/4, 1/4, 1/4). For $BaSrAg_{12}Al_{14}$ the X-ray powder diffraction pattern for the preannealed product contains two separate patterns consistent with the initial products $BaAg_{5.5}Al_{7.5}$ ($a = 12.645(1)$ Å) and $SrAg_{5.5}Al_{7.5}$ ($a = 12.594(3)$ Å). Since these two compounds are isostructural, the two patterns are identical, but each line for $SrAg_{5.5}Al_{7.5}$ appears at a fraction of a degree higher than those lines for $BaAg_{5.5}Al_{7.5}$ as a result of the smaller lattice constant. After annealing the product at 850 °C for 10 days, the powder pattern is consistent with a single-phase product ($a = 12.627(1)$ Å) with Ba and Sr mixed randomly throughout the structure. The results of two single-crystal X-ray diffraction solutions, whose refined compositions were $BaSrAg_{12}Al_{14}$ and $BaSrAg_{12.4}Al_{13.6}$, confirmed these results. Tables 4 and 5 contain information about the single-crystal solution for $BaSrAg_{12}Al_{14}$.

The next three reactions listed in Table 2 (c, d, and e) are all mixtures of one metal which only forms the $NaZn_{13}$ structure, e.g., Ba or Sr, and another which only forms the $ThMn_{12}$ structure, i.e., Y, Dy, or Gd. In all three reactions the products both before and after annealing are multiphase. "$BaYCu_{12}Al_{14}$" (c), as characterized by X-ray powder diffraction, contains a mixture of $BaCu_6Al_7$ and YCu_5Al_7 and was not annealed. "$BaDyCu_{12}Al_{14}$" (d) is also a two-phase product containing both $BaCu_6Al_7$ and $DyCu_5Al_7$ in the preannealed and postannealed (900 °C for 14 days) products. "$SrGdCu_{10}Al_{16}$" (e) is also a mixture of the two phases $SrCu_6Al_7$ and $GdCu_4Al_8$, both before and after annealing (900 °C, 14 days). The annealed products from reactions d and e were analyzed in a JEOL 6100 scanning electron microscope (SEM) using energy dispersive spectroscopy (EDS), and the presence of all four elements in each sample was confirmed by analysis of multiple areas of the sample.

"$SrCeCu_{12}Al_{14}$" (f) was expected to yield similar products as the reactions directly preceding it, as a result of the fact that the ternary $CeCu_xAl_{12-x}$ ($4 < x < 6$) compounds have been reported in the $ThMn_{12}$ structure, and $SrCu_6Al_7$ forms the $NaZn_{13}$ structure. However, a single-phase product, "$SrCeCu_{12}Al_{14}$", containing a random mixture of Sr and Ce atoms was characterized forming the $NaZn_{13}$ structure ($a = 11.980(4)$ Å). This result was confirmed by a single-crystal X-ray solution of a crystal containing a mixture of Sr and Ce atoms.[25,26] The presence of all four elements was confirmed by EDS. The size and valence of these two metal cations are two factors which may contribute to this unexpected result. The ionic radius (CN = 12) of Sr^{2+} is 2.151 Å and of Ce^{3+} is 1.846 Å.[38] Magnetic-susceptibility measurements were carried out on a small sample of $SrCeCu_{12}Al_{14}$, and the material displayed Curie−Weiss paramagnetism with an effective moment of 2.26(1) B.M., which accounts for a nearly 1:1 ratio of Sr:Ce.[26,38] The size difference between Sr^{2+} and Ce^{3+} (0.30 Å) is much smaller than the differences between Ba^{2+} (2.236 Å) and Y^{3+} (1.773 Å) for reaction c and Ba^{2+} and Dy^{3+} (1.775 Å) for reaction d, 0.463 and 0.461 Å, respectively.[38] "$SrGdCu_{10}Al_{16}$" (e), on the other hand, formed a combination of the two ternary compounds, $SrCu_6Al_7$ ($NaZn_{13}$ type) and $GdCu_5Al_7$ ($ThMn_{12}$ type). The similar sizes of Sr^{2+} and Ce^{3+} possibly allow for the mixed occupancy of that position within the $NaZn_{13}$ structure. In a subsequent paper,[26] we examine the factors important for stabilizing the various intermetallic structures $NaZn_{13}$, $ThMn_{12}$, $BaCd_{11}$, and others.

Conclusions

Intermetallic compounds forming the $NaZn_{13}$ type structure resemble Zintl phases in many ways: (1) for a given system there is a narrow range of stable compositions; (2) for the wide range of compounds that form there seems to be a preferred number of 40−42 valence electrons for their existence; (3) in their calculated electronic structures, bonding orbitals are filled and antibonding orbitals are empty, but there is no gap separating these two regions of the spectrum of electronic energy levels. These statements also seem appropriate for Hume−Rothery intermetallics, although similar aspects of their electronic structures are less clear. We are continuing these investigations to provide a strong link between calculated and experimental properties as well as to pursue physical-property measurements of these intermetallics that seem to form a bridge between Hume−Rothery and Zintl compounds.

Supporting Information Available: Tables listing detailed crystallographic data and anisotropic displacement parameters. This material is available free of charge via the Internet at http://pubs.acs.org.

IC980772K

(38) Teatum, E. T.; Gschneidner, K. A., Jr.; Waber, J. T. *Compilation of Calculated Data Useful in Predicting Metallurgical Behavior of the Elements in Binary Alloy Systems*; Los Alamos Scientific Laboratory: New Mexico, 1968.